4*d* and 5*p* photoabsorption in laser-produced thulium plasmas

R. Stefanuik,[1] E. Sokell,[1] E. Long,[1] N. Krstulovic,[1,*] P. Hayden,[1] M. Mahmoad,[2] G. O'Sullivan,[1] and P. Dunne[1]
[1]*School of Physics, University College Dublin, Ireland*
[2]*Institute of Laser for Postgraduate Studies, Baghdad, Iraq*

(Received 27 May 2019; revised manuscript received 16 January 2020; accepted 17 January 2020; published 6 March 2020)

The dual-laser plasma method has been used to record photoabsorption spectra of Tm, Tm^+, and Tm^{2+} ions. The dominant process is 4*d* photoexcitation, giving rise to structure in the 140–240-eV region while structure due to 5*p* excitation is observed in the 27–38-eV region. Due to successive removal of 6*s* electrons outside a $4f^{13}$ core with increasing ionization, the 4*d* photoabsorption spectra of Tm, Tm^+, and Tm^{2+} are very similar. The spectrum of neutral thulium shows autoionizing resonances, excited from both fine-structure levels of the $4f^{13}6s^2$ ground state, evidenced by a clear double-peaked Fano structure in the 140–240-eV range. Similar features are observed and can be associated with 4*d*-4*f* transitions in Tm^+ and Tm^{2+}. Broad structure, distinctly different from the spectra of Tm, Tm^+, and Tm^{2+}, in the same 4*d*-4*f* region of the spectrum at 25 ns suggests that Tm^{3+}, with a different number of 4*f* electrons, may be present in the absorbing plasma immediately after its formation. Significant broadening due to autoionization was observed in the 5*p* absorption region for all three ion stages. The observed transitions were identified with the aid of the COWAN suite of codes, which are based on Hartree-Fock with configuration interaction approach.

DOI: 10.1103/PhysRevA.101.033404

I. INTRODUCTION

The dual-laser plasma (DLP) technique, which uses laser pulses to create separate plasmas that provide both a backlighting continuum and a column of ions that will absorb this continuum, affords a very useful tool to study inner-shell photoabsorption in ions and refractory atoms. By varying either the laser-power density incident on the absorbing plasma or the delay before creating the continuum, it is possible to isolate photoabsorption corresponding to transitions from a number of distinct ion stages. This technique has been successfully applied to study the spectra of a large range of moderately ionized species across the Periodic Table [1], with charge states up to nine times ionized observed [2]. It also provides a method to study atoms and ions of refractory elements, for example, thorium [3]. Early experiments at synchrotrons passed quasimonochromatic synchrotron radiation through furnaces containing vapors of neutral atoms, yielding relative photoabsorption spectra or, when coupled with charged particle detection, relative differential photoionization cross sections [4]. More recent experiments have seen synchrotron radiation merged with an ion beam leading to precise, absolute measurements of photoionization cross sections [5,6]. Emission spectroscopy studies in the vacuum ultraviolet (VUV)–soft x-ray region of the spectrum using laser-produced plasmas [7], electron beam ion traps [8], large-scale plasma devices [9], or collision-based spectroscopy [10] reveal ground and excited-state structure of ions, usually in tandem with atomic structure calculations.

Among the elements in the Periodic Table, thulium is unusual in that the first three members of the isonuclear series have the configuration $4d^{10}4f^{13}6s^n$, where *n* has the value 2, 1, and 0 for Tm, Tm^+, and Tm^{2+}, respectively. This leads to almost identical structure in the 4*d*-4*f* spectra of these species, and some strong similarities in their 5*p*-5*d* spectra, which arises due to the influence of 4*f* wave-function collapse on the atomic structure. Little previous 4*d* photoabsorption work has been undertaken on thulium and this has been limited to studies performed with vapors, which contain only the neutral species in the ground state, $4d^{10}4f^{13}6s^2\ {}^2F_{7/2}$. Photoabsorption measurements were made by Radke [11], who used a furnace to generate an absorbing column of ions, using radiation from the Bonn 500 MeV synchrotron in the 137–206 eV (6–9 nm) region. This study revealed a single strong photoabsorption feature due to excitation of electrons from the $4d^{10}$ inner shell to the 4*f* vacancy originating in the ground state. Since the excited state can autoionize to continuum states it exhibited a broad Fano profile, due to interference between the indirect and direct photoionization processes.

More recently photoelectron measurements have been used to study the same spectral regions in thulium. Kochur *et al.* [12] used term-dependent lifetimes in calculations to reproduce the experimental 4*d* photoelectron spectrum. Additionally, partial cross sections of vaporized neutral thulium in the region of 5*p* excitations were observed by Whitfield *et al.* [4], who also identified discrete and continuum transitions using a customized version of the COWAN Hartree-Fock with configuration interaction (HFCI) simulation code. This yielded a set of experimentally observed and theoretically predicted linewidths, which provide a good baseline for the comparison of both the experimental DLP absorption and the accompanying simulations presented here.

[*]On research leave from Institute of Physics, Bijenicka Cesta 46, 10000 Zagreb, Croatia.

Previous observations of $5p$ photoabsorption in neutral thulium have also been made using furnaces as the source of neutral atoms. The relatively low temperatures of the vapors in these furnaces [typically (∼1,000 K)/(0.1 eV)] once again resulted in absorption only being observed from the lower ($^2F_{7/2}$) level of the $5p^6 4f^{13} 6s^2$ ground state. The $5p$ spectra of Tm I were studied by Tracy [13], who photographically recorded spectra of seven neutral lanthanide elements from Sm ($Z = 62$) to Yb ($Z = 70$) using vapors formed in a furnace as the absorbing species. These were probed by radiation from the Bonn synchrotron between 24 and 36 eV (34–51 nm), revealing a good degree of structure and with assignments made to about 30 features in the photoabsorption spectrum of closed-shell ytterbium. These features were predominantly transitions of the type $5p - nd$, mainly in three series converging on the $5p^5(^2P_{3/2})$ and $5p^5(^2P_{1/2})$ limits. The analysis of the lanthanides from Sm to Tm was less complete, but the spectra showed considerable detail. In particular, the Tm spectrum showed evidence of at least six series built on the $^2P_{3/2}$ and $^2P_{1/2}$ limits. The Tm spectrum is more complicated, due to coupling with the open $4f^{13}$ $^2F_{7/2}$ ground-state configuration. Tracy concluded that the $4f$ and $6s$ electrons essentially play a spectator role during the $5p$ photoabsorption process.

Wernet *et al.* [14] used combined photoelectron spectroscopy with dichroism measurements of the laser-polarized atoms to investigate the $4f$ and $5p$ subvalence photoionization of neutral Tm atoms. The experimental results were compared to Hartree-Fock calculations and again showed that the $5p$ photoelectron spectrum is dominated by the effects of spin-orbit splitting. Whitfield *et al.* [4] observed photoelectron spectra of a thulium vapor created in a furnace at a temperature of 780 °C using undulator radiation passed through a monochromator at the University of Wisconsin Synchrotron. Two analyzers, mounted at 0° and 90° to the direction of polarization of the radiation, allowed the measurement of partial photoelectron cross sections and the β parameters. The pseudo total cross section, created by summing the relative partial cross section for $6s$ and $4f$ photoelectrons, in the region of $5p$ excitation, displayed good agreement with the earlier work of Tracy [13]. The calculations reported by Whitfield *et al.* [4], using a modified version of the atomic structure code of Cowan [15], serve as a good basis for the analysis of $5p$ photoabsorption spectra reported in this work.

In the present work, a laser-produced plasma formed on a solid, planar thulium target was used as a source of absorbing species. This permitted the investigation of photoabsorption in neutral and lowly ionized thulium in two spectral regions, from 140 to 240 eV ($4d$-$4f$) and from 24 to 36 eV ($5p$-$5d$). The observed transitions are interpreted with the aid of calculations carried out using the HFCI codes of Cowan. As a general trend, the level of ionization present in the plasma is seen to decrease, with increasing time delay, in all experiments.

II. EXPERIMENTAL PROCEDURES

The dual-laser plasma technique [1] involves the creation of a line plasma containing the element of interest which then cools and expands on a timescale of hundreds of nanoseconds. During this period of cooling, the level of ionization of the plasma decreases. This allows a particular ion stage to be probed using the continuum emitted from a different laser-produced plasma formed at a controlled time delay, typically between 10 and 2000 ns. The key experimental parameter is the power density of the laser pulses, ϕ. The other control available is the height above the absorbing target at which the continuum probes the plasma. The plasma cools as it expands, leading to a reduced level of ionization further above the target surface during plasma formation and in the initial phase of its expansion [2,16].

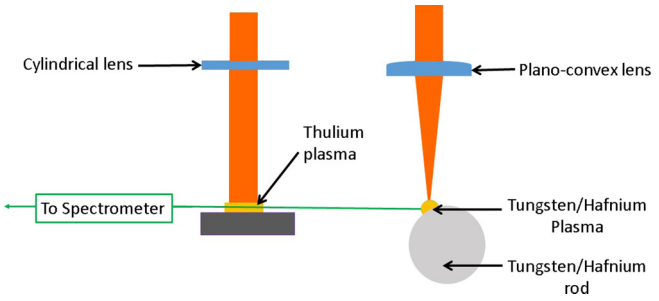

FIG. 1. Schematic diagram of the experimental setup used to record the $5p$-$5d$ and $4d$-$4f$ photoabsorption spectra.

Two different experimental setups, comprising different lasers and spectrometers, were used to record the spectra presented here, due to the layout of the laboratory. Spectra in the 140–240 eV region were recorded on a 0.25-m grazing incidence spectrometer equipped with a variable-line spaced grating with nominal specifications of 1200 grooves per millimeter. The resolving power ($E/\Delta E$) was of the order of 220. Detection was by a 2048 × 2048 pixel back-thinned charge-coupled device (CCD) camera. The output of a Q-switched laser (EKSPLA 512, 5 Hz, 170 ps, max 450 mJ at 1064 nm) was focused tightly onto a planar hafnium target to produce the backlighting continuum source, as hafnium is known to yield an essentially line-free continuum at these wavelengths [17]. The output of a second Nd:YAG laser (Continuum Surelite II, 10 Hz, 6 ns, max 700 mJ at 1064 nm) was focused to form a line plasma containing thulium of length 15 mm and width 1.0 mm via a cylindrical lens. Both plasmas were formed on targets set at the same height, relative to the optical axis of the spectrometer, so that the continuum radiation probed the absorbing plasma along the thulium surface.

To record spectra in the 27–38 eV region the output of a Q-switched laser (Spectron SL805, 10 Hz, 18 ns, max 640 mJ at 1064 nm) was focused tightly onto a rotating tungsten rod to produce the backlighting continuum source, while the output of a second Nd:YAG laser (Continuum Surelite III, 10 Hz, 7 ns, max 270 mJ at 1064 nm) was focused to form a line plasma of length 17 mm and width 1.4 mm on a thulium target via a cylindrical lens. A schematic of both photoabsorption setups is shown in Fig. 1. In the case of the 27–38 eV region, the two plasmas were formed on targets set at different heights, so that the continuum radiation, set at the height of the optical axis of the spectrometer, probed the absorbing plasma along a line located 0.2 mm above the surface of the thulium target. This difference was set to optimize the observed spectra and was measured using a camera to observe both targets. The spectra were recorded using a 1-m normal incidence spectrometer equipped with a 1200 groove per mm platinum-coated grating. The resolving

power of this spectrometer was of the order of 8000. The spectra were detected using a Sony ILX500 linear CCD array, coated with a sodium salicylate phosphor to render it sensitive to VUV radiation. The pixel size was 14 μm in the spectral direction, leading to a spectral resolution of ∼0.14 eV at 30 eV, corresponding to an $E/\Delta E$ of ∼200.

In both experimental configurations, the absorbing plasma conditions were optimized for a particular ion stage using an electronic delay to control the Q switching of the lasers. The time delays ranged from 20 to 2000 ns with timing jitter typically less than 10 ns. To calibrate the wavelength axis of both spectrometers an emission spectrum was taken before each dataset. For the 1-m spectrometer aluminum was used and on the 0.25-m spectrometer reaction-bonded silicon nitride (RBSN) was the reference target yielding spectral lines from silicon and nitrogen in the wavelength region covered by the spectrometer.

III. EXPERIMENTAL RESULTS

In line with the general trend in DLP experiments, the level of ionization present in thulium plasmas is seen to decrease with increasing time delay, in all experiments. In experiments reported in this work on the 1-m spectrometer (5p-5d), neutral species were observed at time delays from 400 ns out to 1900 ns, with higher ion stages being observable at progressively earlier times. In the spectra recorded on the 0.25-m spectrometer (4d-4f) the changes in the photoabsorption profile between 50 and 400 ns, due to 4d excitation, were quite subtle. Beyond 400 ns neutral thulium dominated the spectrum, while at the shortest delays there was evidence for photoabsorption due to triply ionized thulium. In general, neutral and singly ionized species were observed at shorter time delays, typically 50 ns, in the 4d-4f measurements compared

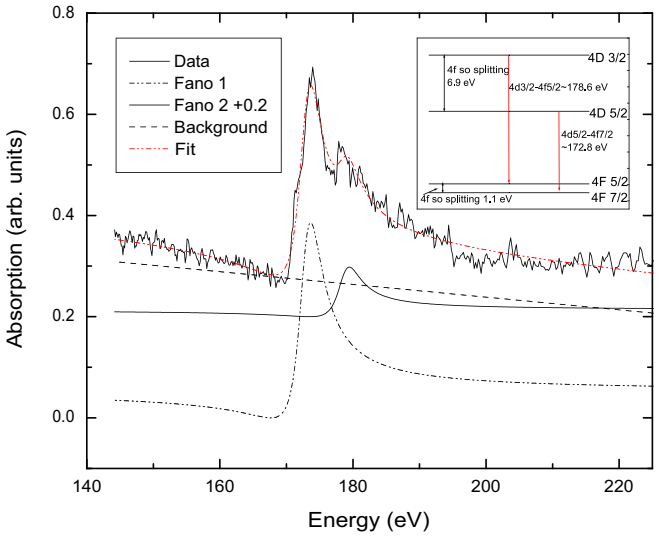

FIG. 2. Photoabsorption spectrum of a thulium plasma, averaged over four shots, recorded at a time delay of 375 ns in the spectral region from 150 to 220 eV. Also shown is the dual Fano profile, including the separate contributions from the two fine-structure components of the 4d-4f transition and the background (dashed line). The inset shows the energies of the two fine-structure components of the 4d-4f transition.

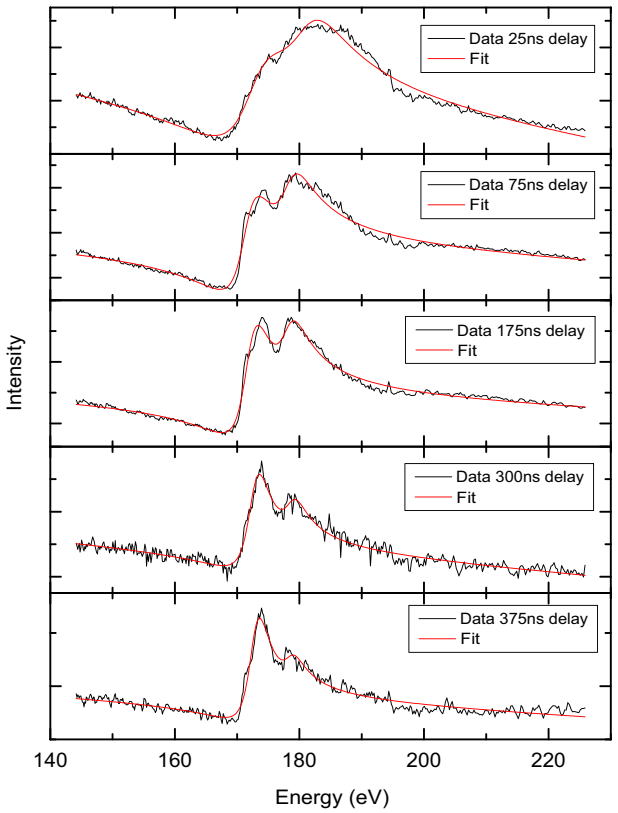

FIG. 3. Photoabsorption spectra of thulium laser plasmas, recorded at time delays of 25–375 ns in the spectral region from 140 to 230 eV. Also shown are the dual Fano profiles fitted as described in the main text. All spectra are the average of four single-shot MEASUREMENTS.

to the delays at which they were observed in the experiments focusing on the 5p-5d spectral region. This difference in the plasma cooling time between the measurements in the two spectral regions may be ascribed to the differences in the experimental arrangements used; a higher power density was employed to generate the absorbing column in the 4d-4f experiments, leading to faster plasma expansion from the surface, and the continuum radiation probed closer to the thulium target surface.

Photoabsorption spectra of thulium in the ∼150-eV to ∼220-eV (4d-4f) spectral region at delays ranging from 25 to 400 ns are shown in Figs. 2 and 3. The strong feature at 173 eV in the spectra recorded at the time delays of 375 ns and longer is that identified first by Radke [11] due to 4d-4f excitation in neutral thulium from the lower $4d^{10}4f^{13}6s^2\ ^2F_{7/2}$ level ($4d^{10}4f^{13}6s^2\ ^2F_{7/2} - 4d^9 4f^{14}6s^2\ ^2D_{5/2}$). The second strong feature in the spectrum, not seen in this earlier work, at approximately 179 eV, is the $4d^{10}4f^{13}6s^2\ ^2F_{5/2} - 4d^9 4f^{14}6s^2\ ^2D_{3/2}$. The latter transition does not appear unless the upper spin-orbit level of the $4f^{13}\,6s^2$ is populated, as is the case in the present laser-produced plasma spectra, but not in the previous studies of Tm vapor. This point is illustrated in the inset of Fig. 2, which shows the two fine-structure components of the 4d-4f transition. Each of the spectra obtained was fitted with a dual Fano profile and background, and these components are shown separately in Fig. 2.

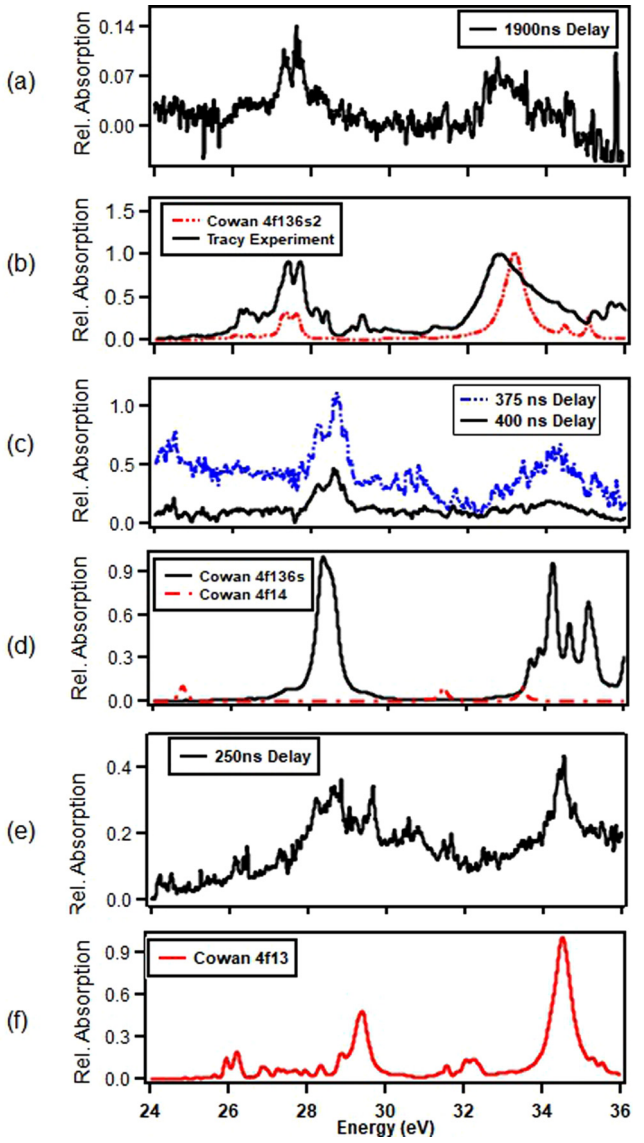

FIG. 4. Photoabsorption spectra of thulium laser plasmas, recorded at time delays of 225–1900 ns in the spectral region from 24 to 38 eV. Also shown for comparison are spectra obtained from previous work (b) [13] and from calculations using the COWAN atomic structure codes (b), neutral, (d) singly ionized, and (f) doubly ionized. The experimental spectra are an average of four or five measurements each averaged over ten shots. A five-point moving average has been applied to the experimental spectra. The synthetic spectra have been shifted as indicated to best fit the experimental data and broadened by convolution, both as described in the text.

Photoabsorption spectra of thulium between 24 and 36 eV at delays ranging from 225 to 1900 ns are shown in Fig. 4. This spectral region displays features arising from $5p$ excitation. These are accompanied by spectra, Fig. 4(b), derived from previous work [13] and simulated spectra derived from atomic structure calculations [15] convolved with Gaussian or Lorentzian functions as appropriate to account for instrumental and lifetime effects, respectively. A consistent evolution in the spectra with increasing time delay is evident.

In the spectrum recorded at a delay of 1900 ns [Fig. 4(a)], strong features at 27.4, 27.7. and a broad feature at 32–33 eV are clearly evident. These were reported in the spectra of neutral thulium by both Whitfield *et al.* [4] and Tracy [13] and it is possible to identify the largest features converging on the $^2P_{3/2}$ and $^2P_{1/2}$ limits, built on the $^2F_{7/2}$ term, with features associated with the $^2P_{3/2}$ limit being around 27 eV. Their separation reflects the spin-orbit splitting of the $5p$ hole state. Weaker features were also observed by Whitfield *et al.* but due to the low signal-to-noise ratio, these are less well defined here. Calculations show that the combined oscillator strength (gf value) associated with the $5p$-$5d$ transitions is about ten times that associated with $5p$-$6d$ transitions. Thus, it is not reasonable to expect to observe any features due to $5p$-$6d$ photoabsorption in this setup.

At shorter time delays, between 400 and 375 ns, a pair of broad intense features at 28.2 and 28.9 eV are observed, together with a broader feature around 34.5 eV, [Fig. 4(c)]. This combination of features becomes weaker at delays below 250 ns and has disappeared by 225 ns. These features are due to the spin-orbit splitting of $5p$-$5d$ photoabsorption in Tm^+ and are analogous to the $5p$-$5d$ transitions seen by Tracy in neutral erbium vapors [13]. Although again the relative intensities of the features associated with the two $5p^{-1}$ thresholds are significantly different in the present spectrum, as for neutral Tm the lower-energy features are much more intense in the DLP spectrum than in Tracy's data.

At a delay of 225 ns [Fig. 4(e)] the spectra show the presence of two features at approximately 29.5- and 34.5 eV. Comparison with calculations shows that these are due to $5p$-$5d$ excitation in Tm^{2+}.

IV. DISCUSSION

Using a collisional radiative model [18] it is possible to estimate the initial electron temperature in the line plasmas used to generate the absorbing species, as ~3.0 eV in the case of the $4d$ datasets and ~2.0 eV for the case of the $5p$ datasets. The electron temperature (in eV) in this model is given by the empirical formula $T_e \approx 5.2 \times 10^{-6} A^{\frac{1}{5}} [\lambda^2 \phi]^{\frac{3}{5}}$, where λ is the wavelength of the laser in μm, A the atomic number, and ϕ is the laser irradiance in W/cm^2. Following the laser pulse, over times ranging from 50 to 2000 ns, laser plasmas are observed to expand and cool, leading to reduced densities and levels of ionization. A survey of earlier experiments reveals a spread of delay times for the appearance of low-charge ion stages. Lysaght *et al.* [19] observed Sn^+ ions in a plasma at a delay of 300 ns and Sn^{3+} at a delay of 60 ns. In the case of gallium plasmas, singly ionized species were observed at a delay of 100 ns and doubly ionized at a delay of 50 ns [20]. In other experiments, Banahan *et al.* [21] observed Pb^{2+} ions and Bi^{3+} ions at delays of 210 and 115 ns, respectively. Some variation in these observations is due to differences in the values of ionization potential among the ions, in the initial power density at the focus of the laser beam used to form the absorbing plasmas, and in the height above the target surface at which the continuum probed the absorbing plasmas.

A. 4*d*-4*f* spectra

Figure 3 clearly indicates the evolution of the photoabsorption profile with increasing time delay. Over this range

of time delays, neutral, singly, and doubly ionized species can be expected to dominate the plasma.

Each of the spectra shown in Fig. 3 was fitted with a dual Fano profile, where the q (Fano parameter) and Γ (linewidth parameter parameters) for the two resonances were constrained to vary in the same way as each other, but the positions and relative strengths were allowed to vary independently along with a linear background. An example of the three components of the fit is shown in Fig. 2. Given the dominate nature of the Fano resonance in the previous work [11], any other contributions to the spectrum were assumed to contribute to the background. For the spectrum recorded at a delay of 375 ns, the separation between the two resonances was determined to be 5.8 ± 0.1 eV. The spin-orbit splitting of both the inner-shell 4d hole and the 4f states determines the splitting of the peaks, given that one transition is from $^2F_{7/2}$ to $^2D_{5/2}$, while the second is $^2F_{5/2}$ to $^2D_{3/2}$. The splitting of the 4f state is given as 1.0875 eV by Meggers [22]. This allows the estimation of the 4d splitting, from the present data, as 6.9 ± 0.1 eV in neutral thulium. The energy level diagram shown in the inset of Fig. 2 demonstrates how this value for the 4d splitting is arrived at.

Over the range of time delays investigated here, neutral, singly, and doubly ionized species can be expected to dominate the plasma. At first inspection, it appears that the 4d-4f excitation barely changes in energy from neutral through doubly ionized thulium, as evidenced by the positions of the main features in the spectra. This may be attributed to the similarities in the electronic structure up to Tm^{2+}. As a result of the removal of 6s electrons with ionization outside a $4f^{13}$ shell, the ground configurations of Tm^+ and Tm^{2+} are $(Xe)4f^{13}(^2F_{7/2})6s$ and $(Xe)4f^{13}(^2F_{7/2})$, respectively. However, the spectra evolve, both in terms of the ratios of the heights of the two main features at ~173 and ~179 eV, and in the width and complexity of those features. The change in the ratio of the heights is due to the increased electron temperature of the plasma at times closer to its formation and the changes in width and profile are due to the variation in the populations of Tm, Tm^+, and Tm^{2+} in the plasmas.

To better evaluate these changes, the difference between the resonance energies fitted to each of the two main features in each of the spectra is plotted against the time delay between 25 and 400 ns in Fig. 5. As the time delay increases, the charge state in the absorbing plasma will reduce. These data suggest that at the two largest delay times shown, neutral Tm is the dominant species in the plasma. For delay times of 400 and 375 ns, the mean value of the energy difference is 5.77 ± 0.12 eV. In the same way as described for the spectrum recorded at 375 ns, this would lead to a slightly improved value of 6.86 ± 0.12 eV for the 4d spin-orbit splitting in neutral Tm.

At slightly shorter delay times, 350 and 300 ns, it might be expected that Tm^+ would become more dominant in the plasma and the small discontinuity observed between 350 and 375 ns in Fig. 4 suggests that the splitting between the two features in Tm^+ may be determined from these data points. The mean energy difference for these two points is 6.04 ± 0.08 eV. The ground-state configuration of Tm^+ allows four levels, $(4f^{13}(^2F_{7/2})6s_{1/2})_4$, $(4f^{13}(^2F_{7/2})6s_{1/2})_3$, $(4f^{13}(^2F_{5/2})6s_{1/2})_2$, and $(4f^{13}(^2F_{5/2})6s_{1/2})_3$, with the average $F_{7/2}$-$F_{5/2}$ splitting being 1.084 eV [23]. This value can be used, in conjunction with the mean value of the resonance separation, to estimate the 4d spin-orbit splitting at 7.12 ± 0.08 eV for Tm^+.

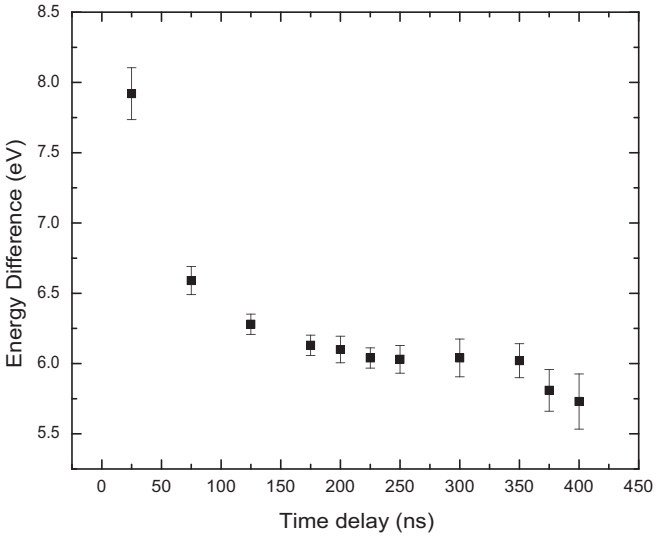

FIG. 5. Plot of the energy differences between the two main features in the 4d-4f photoabsorption spectra as a function of the time delay between the dual-laser pulses.

Between 250 and 225 ns the mean value of the splitting remains at 6.04 ± 0.08 eV, while at 200 and 175 ns it has a mean value of 6.12 ± 0.06 eV. At 125 ns and shorter delays the value of the difference rises steeply, and this is accompanied by an increase in width of the Fano profiles. Similarly, the spin-orbit splitting between the $4f^{13}_{7/2}$ and $4f^{13}_{5/2}$ levels in Tm^{2+} is 1.088 eV [15], giving an estimate of 7.21 ± 0.06 eV for the 4d spin-orbit splitting for this ion, which in this case is simply for two levels. The tendency of the splitting of the 4d fine-structure levels to increase as the charge on the Tm ion increases is also consistent with what would be expected from textbook quantum mechanics [15].

The data in Fig. 5 are interpreted as reflecting the dominant presence of neutral thulium in the plasma at delays of 375 and 400 ns, Tm^+ between 225 and 350 ns, and more tentatively Tm^{2+} between 200 and 150 ns and either excited-state Tm^{2+} or Tm^{3+} at times earlier than 75 ns. Calculations using the COWAN code support this interpretation.

Calculations with the COWAN code, similar to those that supported the identification of the 4d-4f transitions, show that 4d-5f photoabsorption should be observed on the high-energy shoulders of the 173- and 179-eV features, displaced by approximately 0.2 eV. There is evidence for a shoulder on the high-energy side of the features in the spectra shown in Figs. 2 and 3.

Studying the evolution of the spectrum towards shorter time delays reveals features at 175 and 170 eV which may be attributed to excited-state photoabsorption in Tm^{2+}, with absorption from a lower configuration of $(Xe)4f^{12}6s^1$, in contrast to the ground state of $(Xe)4f^{13}$. Spectra recorded at the shortest time delays of 50 and 25 ns show clear evolution of a broad, high-energy shoulder between 185 and 195 eV, which may be due to either the presence of excited

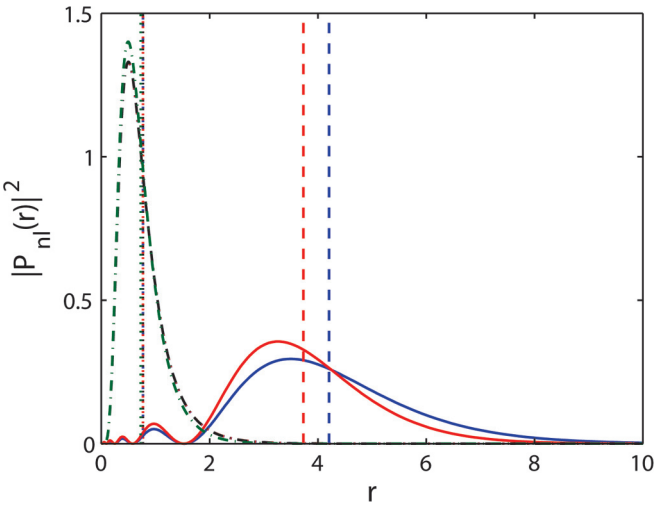

FIG. 6. A plot of the $4f$ (green and black) and $6s$ (blue and red) radial probability distributions for the ground configurations of neutral Tm, Tm^+, Tm^{2+}, and Tm^{3+}. The red and blue lines indicate the $6s$ radial probability distribution for Tm and Tm^+, respectively. The vertical lines highlight the positions of $\langle r \rangle$ for each wave function. The radii are given in atomic units.

Tm^{2+} [configuration $(Xe)4f^{12}6s^1$] or possibly Tm^{3+} ions (configuration $(Xe)4f^{12}$) in the plasma. In each of these cases calculations suggest that the spectra give rise to a far broader spread of lines due to the presence of two vacancies in the $4f$ subshell. The configuration average energy (E_{av}) of the excited state in Tm^{2+} is 6.5 eV above the E_{av} of the ground-state $4d^{10}5s^25p^64f^{13}$.

It is somewhat surprising to see any evidence of triply charged ions in a laser-produced plasma formed with such an initially low electron temperature (~3 eV). According to the collisional radiative model of laser plasmas developed by Colombant and Tonon [18], more than 99% of the Tm will be neutral, singly, or doubly charged. The presence of Tm^{3+} in these plasmas, and indeed the observable photoabsorption contribution from Tm^{2+}, may be connected with the large radial probability distribution of the $6s$ electronic orbital, leading to a large collisional cross section for ionization of neutral, singly ionized, and doubly ionized thulium. While there are no $6s$ electrons in the ground state of doubly ionized Tm, the possibility of Tm^{3+} in the plasma would indeed be evidence for the existence of excited states of Tm^{2+}, having a $6s$ electron more susceptible to collisional ionization. Figure 6 shows a plot of the radial probability densities, determined using the COWAN codes [15], for the $4f$ and $6s$ wave functions in these species. In all cases the $6s$ radial wave function extends well beyond the $4f$, with the average radii being typically four times larger.

B. $4d$-$5p$ spectra

The spectral resolution and dynamic range of the $5p$ spectra, presented in Fig. 4, are inferior to those of Tracy [13]; however, they serve to confirm the presence of specific ions in the plasma under a range of experimental conditions and to allow identification of the main features in the spectra of neutral, singly, and doubly ionized thulium. These spectra clearly show the trend of decreasing ionization with increasing time delay, albeit more slowly than the $4d$-$4f$ spectra. The increased delays arise due to the lower initial power density of the laser pulses forming the absorbing plasma, leading to a slower expansion velocity, and the fact that the continuum probed the absorbing plasma 0.2 mm above the target surface in this case. It is worth noting that Tracy presented composite scans, using high vapor density for regions of low photoabsorption cross section and low vapor density for regions of larger cross section. In the present work the vertical shifting within spectra necessitated by this use of different vapor densities is not required.

Analysis of the absorption spectra was aided by HFCI COWAN calculations [15] for each of the ion stages present at different time delays. The calculations also accounted for the increased widths of the observed transitions resulting from autoionization, as the transition energies lie well above the ionization potential of neutral thulium, which is 6.184 eV [23].

The following transitions for neutral Tm were included in the calculations: $5p^64f^{13}6s^2$–$5p^54f^{13}6s^2ms, nd$ with $6 < m < 11$ and $4 < n < 11$. These resonances were chosen to be consistent with the previous work of Whitfield *et al.* [4] and to allow for any effects due to configuration interaction. Similarly following the work of Whitfield *et al.*, the Slater integrals were scaled by 80% from their *ab initio* calculations, with the exception of the spin-orbit integral which was left unscaled. The calculated oscillator strengths were seen to decrease significantly with increased m and n values. To account for autoionization, the following routes to Tm^+ states were considered for the decay of $5d$ states located in the continuum:

$$\begin{aligned} 5p^54f^{13}6s^25d &\rightarrow 5p^64f^{13}6s + \varepsilon l (l = 1, 3) \\ &\rightarrow 5p^64f^{12}6s^2 + \varepsilon l (l = 0, 2) \\ &\rightarrow 5p^64f^{13}5d + \varepsilon l (l = 1, 3) \\ &\rightarrow 5p^64f^{12}6s5d + \varepsilon l (l = 0, 2) \\ &\rightarrow 5p^64f^{11}6s^25d + \varepsilon l (l = 1, 3). \end{aligned}$$

Here ε is the kinetic energy of the ionized electron and l is the angular momentum of the ionized electron. Transitions were then convolved with either a Gaussian or a Lorentzian depending on the linewidth. If the linewidth was equal to or lower than the approximate experimental width, then the line was considered instrumentally broadened (by 0.136 eV) and was convolved with a Gaussian function. If the linewidth was greater than 0.136 eV, then the line was convolved with a Lorentzian which had a full width at half maximum (FWHM) intensity equal to the calculated linewidth of the transition. The synthetic spectrum was shifted by ~+0.318 eV to best agree with the experimental spectrum [Figs. 4(a) and 4(b)], which it does. However, the simulated intensity for the higher-energy feature is significantly greater than that for the lower-energy sharper features at ~27 eV; in Tracy's experimental spectrum the higher-energy feature is slightly more intense than the features at ~27 eV [13]. This relative intensity is at odds with the present experimental spectrum. Whitfield *et al.* [4] presented pseudo total absorption cross section spectra (generated from summing the state-specific constant ion state spectra that they recorded), which also shows the

lower-energy features as being more intense than the broad feature at ∼32 eV. Furthermore, the theoretical spectrum, compared with the pseudo total absorption cross section spectra has a feature at ∼32 eV which is also less intense than those at ∼27 eV [4]. This theoretical spectrum was generated using Cowan's code in combination with routines to generate synthetic spectra based on Mies' formalism for photoionization [24], to account for the calculated broadening and the effect of overlapping resonances [25]. This work suggests that the relative intensities observed in the present experimental spectrum are credible and the present overestimation of the intensity of the feature at ∼32 eV in the synthetic spectrum results from effects not included in the present simulations.

The agreement between the DLP spectrum and the COWAN calculations for Tm^+, shown in Figs. 4(c) and 4(d), is reasonable. The following transitions were included in the COWAN code calculations: $5p^64f^{13}6s^1$–$5p^54f^{13}6s^1ms,\ nd$ with $6 < m < 10$ and $5 < n < 10$ and the Slater integrals were scaled to 80% of their *ab initio* values, with the exception of the spin-orbit integral which was left unscaled. The synthetic spectrum was shifted by +0.469 eV to best fit the experimental spectrum. The same convolution procedure was used for Tm^+ as for the neutral, described above. The excited $5p^54f^{13}6s^15d^1$, $5p^54f^{13}6s^2$, $5p^54f^{13}6s^16d^1$, $5p^54f^{13}6s^17s^1$, and $5p^54f^{13}6s^17d^1$ configurations are estimated to lie at 3.42, 5.49, 6.43, 12.33, and 13.49 eV above the ionization potential of Tm^+, respectively. Hence, the influence of autoionization on the widths of the photoabsorption transitions to states in these configurations was calculated. The following decay channels for 5d states were included in the calculations:

$$\begin{aligned} 5p^54f^{13}6s5d &\rightarrow 5p^64f^{13} + \varepsilon l(l = 1, 3) \\ &\rightarrow 5p^64f^{12}nd + \varepsilon l(l = 0, 2) \\ &\rightarrow 5p^64f^{12}6s + \varepsilon l(l = 0, 2). \end{aligned}$$

In addition, the following decay channels for 6s states were included:

$$\begin{aligned} 5p^54f^{13}6s^2 &\rightarrow 5p^64f^{13} + \varepsilon l(l = 1, 3) \\ &\rightarrow 5p^64f^{12}ms + \varepsilon l(l = 0, 2). \end{aligned}$$

As the thulium ions are created in a laser-produced plasma, absorption from the excited terms, $(4f^{13}(^2F_{7/2})6s_{1/2})_3$, $(4f^{13}(^2F_{5/2})6s_{1/2})_2$, and $(4f^{13}(^2F_{5/2})6s_{1/2})_3$, are all likely and are included in the calculations. In addition, conditions to support a population of the excited configuration $5p^64f^{14}$ which lies 6.9 eV above the ground state are expected to exist in the absorbing plasma. Features due to absorption from the $5p^64f^{14}$ state are predicted to lie at 24.3 eV and between 31 and 34.5 eV, which can be seen in the spectrum recorded at a delay of 375 ns, shown in Figs. 4(c) and 4(d). For simulation of these excited states, the following transitions were included in the COWAN code calculations: $5p^64f^{14}$–$5p^54f^{14}ms,nd$ with $6 < m < 10$ and $5 < n < 10$ and the Slater integrals were scaled to 80% of their *ab initio* values, with the exception of the spin-orbit integral which was left unscaled. Only one autoionizing decay channel for 5d states was included in the calculations as all others lay below the ionization threshold:

$$5p^54f^{14}5d \rightarrow 5p^64f^{13} + \varepsilon l(l = 0, 2).$$

In addition, the following decay channels for 6s states were included:

$$\begin{aligned} 5p^54f^{14}6s &\rightarrow 5p^64f^{13} + \varepsilon l(l = 0, 2) \\ &\rightarrow 5p^64f^{12}6s + \varepsilon l(l = 1, 3). \end{aligned}$$

As the delay between the formation of the thulium plasma and the continuum-emitting plasma is reduced to 225 ns, strong features arise in the spectra, which are not attributable to photoabsorption in singly ionized thulium, but which can be assigned to 5p photoabsorption in doubly ionized thulium. These features persist in spectra recorded between the delays of 175 and 150 ns. The DLP spectrum shown in Fig. 4(e), recorded at a delay time of 250 ns, is quite consistent with the Tm^{2+} synthetic spectrum shown in the upper part which was shifted by +0.587 eV. The DLP spectrum in the 5p excitation region was recorded at an absorbing plasma temperature of ∼2 eV, at which a significant population of Tm^{2+} ions is not likely to occur [18]. However, as in the case of the 4d-4f spectra, the large radius of the 6s wave function (Fig. 6) may increase the possibility of producing Tm^{2+} in these plasmas. Strong features due to 5p-5d transitions in Tm^{2+} are seen at 29.6 and 34.5 eV. These were identified with the aid of calculations using the COWAN suite of codes for transitions in Tm^{2+}, which included the following configurations: $5p^64f^{13}$–$5p^54f^{13}ms,\ nd$ with $6 < m < 10$ and $5 < n < 10$. The Slater Integrals were scaled to 85% of their *ab initio* values, with the exception of the spin-orbit integral, which was again unscaled, to best match the observed 5p spin-orbit splitting of 4.9 eV. The output was again convolved in the manner described above for neutral Tm. The following decay channel for 5d states was included in the calculations:

$$5p^54f^{13}5d \rightarrow 5p^64f^{12} + \varepsilon l(l = 0, 2).$$

V. CONCLUSIONS

Using the dual-laser plasma technique photoabsorption spectra of plasmas containing thulium have been observed in two energy regions. Neutral and lowly ionized Tm are spectroscopically interesting because of their single 4f vacancy. As transitions involving the 6s electrons do not contribute to the spectra significantly, Tm^+ and Tm^{2+} have similar spectra, although these species have not been thoroughly studied experimentally before. Due to the range of plasma temperatures studied features due to 4d-4f and 5p-5d excitation were observed in ions from neutral Tm to Tm^{2+}. Features were identified with the aid of atomic structure calculations and by isolating ion stages as a function of absorbing plasma temperature. The evolution of 4d-4f photoabsorption of Tm, Tm^+, and Tm^{2+} was successfully studied via the behavior of a double-peaked Fano profile, a feature uniquely observable using the DLP technique due to the significant population of the $4d^{10}4f^{13}6s^2\ ^2F_{5/2}$ excited state in neutral thulium and analogous states in Tm^+ and Tm^{2+}. Spectral changes are subtle in this spectral region; hence the evolution of the ion states was inferred from the changes in the line separation and linewidths as a function of time delay.

As the plasmas contain species other than the lowest spin-orbit component of the ground state, transitions in neutral Tm that have not previously been experimentally observed

have been studied in the region of $5p$ excitation. The $5p$-$5d$ transitions originating in the metastable $4f^{14}$ configuration for Tm^+ have also been identified in the spectra. Thulium ions are present in the laser plasmas at laser power densities and plasma temperatures below those normally expected to lead to significant ionization. This is attributed to the large radial size of the $6s$ wave function, leading to enhanced collisional ionization rates even at low plasma temperatures.

ACKNOWLEDGMENTS

Support from Science Foundation Ireland (SFI) is acknowledged under Grant No. 08/RFP/PHY1180. P.H. acknowledges support from SFI under its Starter Investigator Research Grant (SIRG) Programme 2013, Grant No. 13/SIRG/2100. E.L. acknowledges support from The Irish Research Council Enterprise Partnership Scheme Postgraduate Scholarship No. EPSPG/2012/422.

[1] J. T. Costello, J. P. Mosnier, E. T. Kenndey, K. P Carroll, and G. O'Sullivan, Phys. Scr. **T34**, 77 (1990).

[2] L. Gaynor, N. Murphy, P. Dunne, and G. O'Sullivan, J. Phys. B: At. Mol. Opt. Phys. **41**, 245002 (2008).

[3] P. K. Carroll and J. T. Costello, Phys. Rev. Lett. **57**, 1581 (1986).

[4] S. B. Whitfield, K. Caspary, R. Wehlitz, and M. Martins, J. Phys. B: At. Mol. Opt. Phys. **41**, 015001 (2008).

[5] E. T. Kennedy, J. P. Monier, P. van Kampen, D. Cubaynes, S. Guilbaud, C. Blancard, B. M. McLaughlin, and J.-M. Bizau, Phys. Rev. A **90**, 063409 (2014).

[6] S. Schippers, T. Buhr, A. Borovik, Jr., K. Holste, A. Perry-Sassmannshausen, K. Mertens, S. Reinwardt, M. Martins, S. Klumpp, K. Schubert, S. Bari, R. Beerwerth, S. Frizsche, S. Ricz, J. Hellhund, and A. Muller, X-Ray Spectrom. **49**, 11 (2019).

[7] T. Wu, T. Higashiguchi, B. Li, G. Arai, H. Hara, Y. Kondo, T. Miyazaki, T.-H. Dinh, P. Dunne, F. O'Reilly, E. Sokell, and G. O'Sullivan, J. Phys. B: At. Mol. Opt. Phys. **49**, 035001 (2016).

[8] K. Fahy, P. Dunne, L. McKinney, G. O'Sullivan, E. Sokell, J. K. White, A. Aguilar, J. M. Pomeroy, J. N. Tan, B. Blagojevi, E.-O. LeBigot, and J. D. Gillaspy, J. Phys. D: Appl. Phys. **37**, 3225 (2004).

[9] C. Suzuki, F. Koike, I. Murakami, N. Tamura, S. Sudo, and G. O'Sullivan, Atoms **7**, 66 (2019).

[10] H. Ohashi, H. Tanuma, S. Fujioka, H. Nishimura, A. Sasaki, and K. Nishihara, J. Phys.: Conf. Ser. **58**, 235 (2007).

[11] E. R. Radke, J. Phys. B: At. Mol. Opt. Phys. **12**, L71 (1979).

[12] A. G. Kochur, I. D. Petro, J. Schulz, and Ph. Wernet, J. Phys. B: At. Mol. Opt. Phys. **41**, 215002 (2008).

[13] D. H. Tracy, Proc. R. Soc. Lond. A. **357**, 485 (1977).

[14] Ph. Wernet, A. Verweyen, J. Schulz, B. Sonntag, K. Godehusen, R. Muller, P. Zimmermann, and M. Martins, J. Phys. B: At. Mol. Opt. Phys. **35**, 3887 (2002).

[15] R. D. Cowan, *The Theory of Atomic Structure and Spectra* (University of California Press, Berkeley, CA, 1991).

[16] L. Gaynor, N. Murphy, D. Kilbane, A. Cummings, G. O'Sullivan, J. T. Costello, P. van Kampen, and E. T. Kennedy, J. Phys. B: At. Mol. Opt. Phys. **38**, 2895 (2005).

[17] P. K. Carroll, E. T. Kennedy, and G. O'Sullivan, Appl. Opt. **19**, 1454 (1980).

[18] D. Colombant and G. F. Tonon, J. Appl. Phys. **44**, 3524 (1973).

[19] M. Lysaght, D. Kilbane, N. Murphy, A. Cummings, P. Dunne, and G. O'Sullivan, Phys. Rev. A **72**, 014502 (2005).

[20] P. Dunne, G. O'Sullivan, and V. K. Ivanov, Phys. Rev A **48**, 4358 (1993).

[21] C. Banahan, C. McGuinness, J. T. Costello, D. Kilbane, J-P. Mosnier, E. T. Kennedy, G. O'Sullivan, and P. van Kampen, J. Phys. B: At. Mol. Opt. Phys. **41**, 205001 (2008).

[22] W. F. Meggers, Rev. Mod. Phys. **14**, 96 (1942).

[23] W. C. Martin, Z. Zalubus, and L. Hagan, *Atomic Energy Levels: The Rare Earth Elements*, National Bureau of Standards NSRDS-NBS 60 (U.S. Department of Commerce, Washington, DC, 1978).

[24] F. Mies, Phys. Rev. **175**, 164 (1968).

[25] M. Martins, J. Phys. B: At. Mol. Opt. Phys. **34**, 1321 (2001).